ACS APPLIED MATERIALS & INTERFACES

Research Article

www.acsami.org

One-Step Preparation of a Water-Soluble Carbon Nanohorn/Phthalocyanine Hybrid for Dual-Modality Photothermal and Photodynamic Therapy

Bang-Ping Jiang,[†,‡] Lan-Fang Hu,[†,‡] Xing-Can Shen,[*,†] Shi-Chen Ji,[†] Zujin Shi,[§] Chan-Juan Liu,[†,▽] Li Zhang,[†] and Hong Liang[*,†]

[†]Ministry of Education Key Laboratory for the Chemistry and Molecular Engineering of Medicinal Resources, School of Chemistry and Pharmaceutical Science, Guangxi Normal University, Guilin 541004, People's Republic of China

[§]Beijing National Laboratory for Molecular Sciences, College of Chemistry and Molecular Engineering, Peking University, Beijing 100871, People's Republic of China

[▽]Key Laboratory of New Processing Technology for Nonferrous Metal & Materials, Ministry of Education, School of Material Science and Engineering, Guilin University of Technology, Guilin 541004, People's Republic of China

Supporting Information

ABSTRACT: The biomedical applications of carbon nanomaterials, especially integrating noninvasive photothermal therapy (PTT) and photodynamic therapy (PDT), into a single system have enormous potential in cancer therapy. Herein, we present a novel and facile one-step method for the preparation of water-soluble single-walled carbon nanohorns (SWNHs) and metal phthalocyanines (MPc) hybrid for PTT and PDT. The hydrophilic MPc, tetrasulfonic acid tetrasodium salt copper phthalocyanine (TSCuPc), is coated on the surface of SWNHs via noncovalent $\pi-\pi$ interaction using the sonication method. In this PTT/PDT nanosystem, SWNHs acts as a photosensitizer carrier and PTT agent, while TSCuPc acts as a hydrophilic and PDT agent. The EPR results demonstrated that the generated reactive oxygen species (ROS) not only from the photoinduced electron transfer process from TSCuPc to SWNHs but also from SWNHs without exciting TSCuPc to its excited state. The test of photothermal conversion proved that not only do SWNHs contribute to the photothermal therapy (PTT) effect, TSCuPc probably also contributes to that when it coats on the surface of SWNHs upon exposure to a 650-nm laser. More importantly, the results of *in vitro* cell viability revealed a significantly enhanced anticancer efficacy of combined noninvasive PTT/PDT, indicating that the SWNHs–TSCuPc nanohybrid is a hopeful candidate material for developing an efficient and biocompatible nanoplatform for biomedical application.

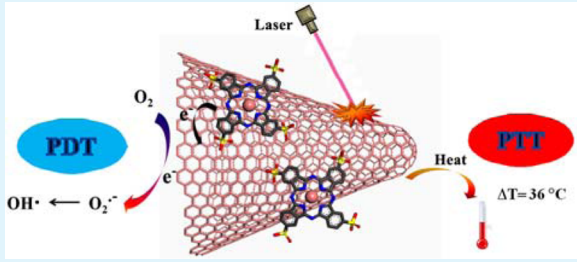

KEYWORDS: *single-walled carbon nanohorns, metal phthalocyanine, photothermal therapy, photodynamic therapy*

1. INTRODUCTION

Carbon nanomaterials, including graphene, single-walled carbon nanohorns (SWNHs), and single-walled carbon nanotubes (SWNTs), have attracted tremendously scientific attention and wide applications in the past decade, because of their unique physical and chemical propeties.[1−10] SWNHs, originally reported by Iijima et al. in 1999,[11] are horn-shaped nanostructures with an average cone angle of 120°, a diameter of 2−5 nm, and a length of 40−50 nm, forming a round-shaped aggregates of 50−100 nm in diameter.[10−13] This diameter is in the optimal size range for the enhanced permeability and retention (EPR) effect for their accmulation at the tumor site.[14,15] In contrast to SWNTs, SWNHs contain no metal impurity, because the synthesis of SWNHs is through laser ablation or arc discharge using pure graphite rods without any metal catalysts.[12,13] Therefore, SWNHs have negligible toxicity, both *in vitro* and *in vivo*,[14,15] which facilitates the fabrication of the functionalized nanoplatforms for biomedical applications with low toxicity. Furthermore, similar to other carbon nanomaterials, such as fullerene,[16] graphene (GR),[17] and SWNTs,[18] SWNHs can also act as a promising photothermal agent and efficiently convert infrared or near-infrared (NIR) light into heat, thus resulting in hyperthermia to cells and surrounding tissue.[14,19,20]

Photothermal therapy (PTT) is a form of phototherapy, which results in irreversible cell damage by heating the targeted tissue for minutes through the conversion of energy absorbed from photons by a PTT agent.[14,16−20] Photodynamic therapy (PDT) is another type of phototherapy method. In the process of PDT, a photosensitizer (PS) selectively absorbs a particular wavelength of light, and then produces reactive oxygen species (ROS) such as singlet oxygen ($^1O_2$) or free radicals by

Received: July 23, 2014
Accepted: September 23, 2014
Published: September 23, 2014

transferring the photon energy to surrounding oxygen molecules, which can cause the death of cancer cells.[21−23] Metal phthalocyanines (MPc), which are two-dimensional (2D) 18-π-electron aromatic macrocycles with a metal coordination at the central cavity, have widely acted as PS agents for PDT.[24] However, since the severe self-aggregation of MPc in aqueous environments leads to the loss of ROS generation efficiency, their applications for PDT are restricted in physiological environments. The bonding MPc on the surface of nanomaterials is an efficacious strategy not only for reduction the self-aggregation of MPc, but also used to fabricate the functionalized nanoplatforms.[25]

Currently, combination therapies of nanoplatforms for cancer treatment are receiving more and more attention.[14,19,23] The combinations of noninvasive PTT and PDT into a single system have been explored intensively in recent years, because of their enhanced therapeutic efficiency and reduced side effects, relative to the individual therapeutic response.[23] For example, a PDT−PTT double therapy system has been developed, in which zinc phthalocyanine (ZnPc) was loaded inside the oxidized SWNHs (SWNHox) with surface opened holes, and the protein bovine serum albumin (BSA) was attached to the carboxyl groups of SWNHox. Such prepared ZnPc−SWNHox−BSA provided an exciting opportunity for both PDT and PTT.[19,20] However, the preparation methods in this system and other multifunctional nanocarbon systems are often relatively complex and require multiple steps, generally including oxidization of carbon nanomaterials, loading the conjugated PS or other drug molecules, and the grafting hydrophilic agent to improve water solubility, which may lead to inferior physical properties and reduce the electrical conductivity of carbon nanomaterials.[16−20,23] Thereby, facile methods are required to obtain both the multifunctions and the water solubility of carbon nanoplatforms, while retaining the desirable intrinsic properties of nanocarbon at the same time.

Tetrasulfonic acid tetrasodium salt copper phthalocyanine (TSCuPc) is one type of water-soluble MPc. The recently studies have showed that noncovalent $\pi-\pi$ stacking interaction can load the TSCuPc on carbon nanomaterials. Hatton et al. reported that the dispersions of surface-oxidized multiwall carbon nanotubes (*o*-MWCNTs) in aqueous solutions of TSCuPc are stable.[26] Fan et al. developed the TSCuPc-functionalized carbon nanotubes to support Pd nanoparticles for enhanced formic acid electro-oxidation.[27] Recently, our group reported the TSCuPc-functionalized graphene for fabrication of the novel fuel cell and glucose biosensor.[28,29] Chunder et al. have studied the reduced graphene oxide/TSCuPc composite and its optoelectrical properties.[30] Inspired by these studies, it is supposed that, with a high and accessible π-electron surface, SWNHs are feasible to load TSCuPc directly to obtain functionality and high water dispersity. However, to the best of our knowledge, TSCuPc-functionalized SWNHs through interfacial noncovalent $\pi-\pi$ stacking have not yet been reported.

Herein, we attempt to fabricate a SWNHs−TSCuPc nanohybrid for both PTT and PDT via a facile one-step method of sonication. The hydrophilic TSCuPc bring the water-solubility to SWNHs−TSCuPc nanohybrid without oxidization and further surface modification. The synergistic effect of both PTT and PDT is revealed in the SWNHs−TSCuPc nanohybrid. Especially, the as-prepared SWNHs−TSCuPc nanohybrid exhibits enhanced anticancer efficacy *in vitro*, which may be a potential dual-modality nanoplatform for biomedical application.

2. MATERIALS AND EXPERIMENTS

Materials. The SWNHs was produced by direct current arc-discharge between pure graphite rods in air atmosphere without using any metal catalysts.[13] Copper(II) phthalocyanine−3,4′,4″,4‴-tetrasulfonic acid tetrasodium salt (TSCuPc), 5,5-dimethyl-1-pyrroline-*N*-oxide and propidium iodide (PI) were purchased from Aldrich. Calcein AM was obtained from Tianjin Biolite Biotech., Inc. (Tianjin, China). All above chemicals were used directly without further purification.

Preparation of SWNHs-TSCuPc Nanohybrid. SWNHs (10 mg) were added to an aqueous solution of TSCuPc (40 mL, 0.5 mg mL^{-1}), followed by sonication at a power output of 140 W for 3 h. Subsequently, the dispersion was centrifuged at 5000 rpm for 30 min to remove larger aggregates, and the inklike supernatant was collected. After that, the resultant inklike solution was filtered through a 0.22 μm polytetrafluoroethylene (PTFE) membrane filter and rinsed with water until the filtrate became colorless, ensuring that no free TSCuPc existed in the precipitate. Finally, the precipitate was redissolved in pure water, which was found to be stable for months as the SWNHs−TSCuPc nanohybrid.

Characterizations and Instruments. The morphologies of SWNHs−TSCuPc were studied by transmission electron microscope (TEM, Model H-600, JEOL, Japan). The ultraviolet−visible (UV-vis) spectra were recorded on a Cary 100 UV−visible spectrometer. The Raman spectra were measured on a Renishaw inVia Raman microscope at a 514-nm exciting line, which were taken with exposure times of 10 s and 30% power at 20 times of accumulation. X-ray photoelectron spectra (XPS) were obtained with an ESCALAB 250 spectrometer with a monochromatic Al Kα (1486.6 eV) X-ray source. Survey and high-resolution spectra were recorded at pass energy of the analyzer of 150 and 20 eV, respectively. The binding energies were calibrated to the C 1s binding energy of contamination carbon at 284.8 eV. High-resolution spectra were deconvoluted with the Gaussian−Lorentzian mixed function after background subtraction with the Shirley method using the software "XPS peak". Atomic ratios were computed from experimental intensity ratios and normalized by atomic sensitivity factors. TGA (Labsys Evo; Setaram Instruments) was carried out in nitrogen gas at a temperature elevation rate of 10 °C/min.

Photothermal Effect Measurement. SWNHs−TSCuPc and TSCuPc solutions were diluted to a final concentration of 10 μg mL^{-1} of TSCuPc equivalent, and the corresponding amount of SWNHs in SWNHs−TSCuPc was 16.5 μg mL^{-1}. One milliliter (1 mL) of these solutions was placed in a series of specimen bottles and each bottle was irradiated by a 650-nm laser (3 W cm^{-2}). Light-induced temperature change in the solutions were collected every 30 s by using a thermal camera (MAG30, Magnity Electronics, China).

Reactive Oxygen Species Generation. The generation of singlet oxygen by free TSCuPc and SWNHs−TSCuPc was detected using anthracene-9,10-dipropionic acid disodium salt (ADPA) as the indicator. A quantity of 150 μL of ADPA solution (100 mM) was added to 2 mLof TSCuPc or SWNHs−TSCuPc solution, and was irradiated with a 650-nm laser (3 W cm^{-2}) or an 808-nm laser (3 W cm^{-2}). After irradiation for special time, the fluorescence intensity of ADPA (λ_{exc} = 376 nm) were measured by time-resolved fluorescence spectroscopy (FL3-P-TCSPS, Horiba Jobin Jvon, France).

To measure the generation of $O_2^{\bullet -}$ or $OH^{\bullet}$ by SWNHs–TSCuPc, 5,5-dimethyl-1-pyrroline-*N*-oxide (DMPO) was used as a spin trap reagent. Experimental solution was prepared by mixing 10 μL of the SWNHs–TSCuPc nanohybrid (TSCuPc, 100 μg mL^{-1}; SWNHs, 165 μg mL^{-1}), 10 μL DMPO (0.8 M), and 80 μL PBS (pH 7.0). The solution was placed in a quartz cell and irradiated with a 650-nm laser (3 W cm^{-2}) or an 808-nm laser (3 W cm^{-2}) for 5 min. After that, the solution was inserted into a capillary tube and then placed in the EPR cavity, and the spectra were recorded on a Bruker Model A300 spectrometer at 298 K. The measurement parameters were as follows: frequency, 9.8 GHz; microwave power, 19.87 mW; sweep time, 27.65 s; sweep width, 200 G; modulation frequency, 100 kHz.

Phototherapy Assay. The *in vitro* cytotoxicity study was performed using human cervical cancer cells (HeLa cells). Cells were cultured in normal RPMI-1640 culture medium containing 10% fetal bovine serum and 1% penicillin-streptomycin at 37 °C under 5% CO_2. For cytotoxicity assay, HeLa cells were seeded into 96-well cell-plates with 10^4 cells per well and incubated at 37 °C for 24 h. Then, the cells were treated with free TSCuPc or SWNHs–TSCuPc nanohybrid at a series of concentrations for 24 h. During this time, cells were kept in darkness, without light exposure. After that, 10 μL of methyl thiazolyl tetrazolium (MTT) solution was added to each well and the plate was incubated for another 2 h. The intracellular formazan crystals were extracted into 100 μL of DMSO after removing the medium, and then the optical density (OD) at 570 nm was recorded by a microplate reader.

To measure the phototoxicity, cells were seeded as previously done. After 24 h of incubation, cells were treated with free TSCuPc or SWNHs–TSCuPc nanohybrid at a series of concentrations (TSCuPc, 0–15 μg mL^{-1}; SWNHs, 0–26.5 μg mL^{-1}) for 24 h. Then, cells were irradiated with a 650-nm laser (3 W cm^{-2}). The cells were incubated for another 24 h and cell viabilities were measured by standard MTT assay. In addition, the phototoxicity at different irradiation times was determined as follows: first, cells were treated with fixed concentrations of free TSCuPc or SWNHs–TSCuPc nanohybrid (TSCuPc, 10 μg mL^{-1}; SWNHs, 16.5 μg mL^{-1}) for 24 h; second, cells were irradiated with a 650-nm laser (3 W cm^{-2}) for various times; finally, the cells were incubated for another 24 h and cell viabilities were measured by standard MTT assay.

The cell viability was estimated according to the following equation:

$$\text{cell viability}\,[\%] = \left(\frac{\text{OD}_{\text{treated}}}{\text{OD}_{\text{control}}}\right) \times 100$$

where the OD represented optical density, and PBS-added samples without laser irradiation were set as the control.

Confocal Microscopy Measurement. HeLa cells were cultured with the solution of SWNHs–TSCuPc nanohybrid (TSCuPc, 10 μg mL^{-1}; SWNHs, 16.5 μg mL^{-1}) in 24-well microplates at a density 1 × 10^5 cells mL^{-1} per well for 24 h. Then, the HeLa cells were washed with PBS three times to remove the unadsorbed SWNHs–TSCuPc nanohybrid. Calcein AM (2 μM) and PI (4 μM) were added into cells and stained for 20 min, and then the cells were irradiated with a 650-nm laser for 15 min (3 W cm^{-2}). The confocal images were taken by a confocal laser microscope (Karl Zeiss Model LSM 710, Jena, Germany). HeLa cells treated with PBS buffer solution were used as a control.

3. RESULTS AND DISCUSSION

Synthesis and Characterization of the SWNHs–TSCuPc Nanohybrid. SWNHs–TSCuPc nanohybrid was fabricated by noncovalently coating TSCuPc on the surface of SWNHs via a facile one-step method of sonication, as depicted in Scheme 1. An intuitive comparison between SWNHs, TSCuPc, and SWNHs–TSCuPc nanohybrid is represented in the photograph shown in Figure 1 (inset). The high solubility of SWNHs into aqueous solution suggests that the surface of SWNHs is covered by TSCuPc.

Scheme 1. Schematic Illustration of the Preparation of the SWNHs–TSCuPc Nanohybrid (Counterions Are Omitted for the Sake of Clarity)

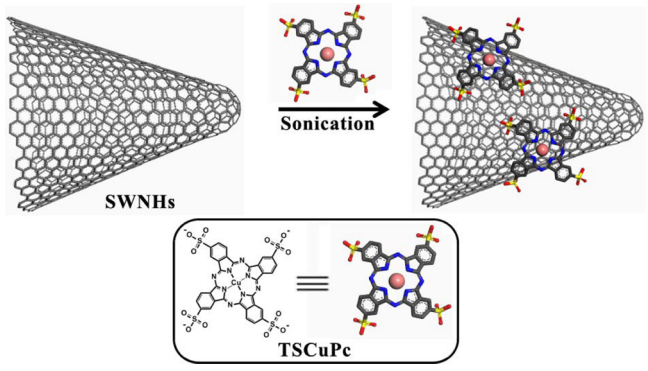

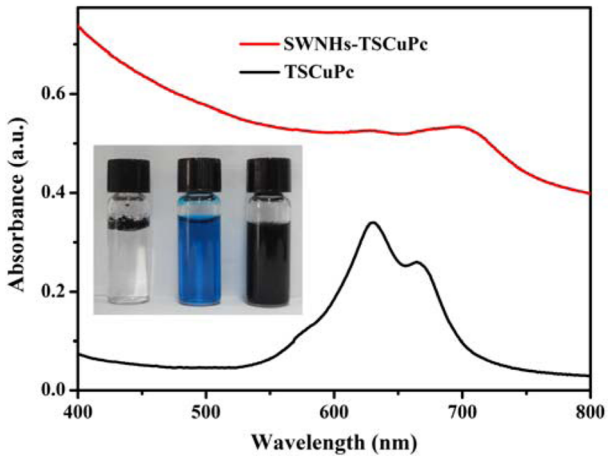

Figure 1. UV–vis spectra of TSCuPc (TSCuPc, 5 μg mL^{-1}) and SWNHs–TSCuPc nanohybrid (TSCuPc, 5 μg mL^{-1}; SWNHs, 8.8 μg mL^{-1}) in aqueous solution. Inset shows a photograph of SWNH (left), TSCuPc (middle), and SWNHs–TSCuPc (right) dispersed in water.

We evaluated UV–vis spectra of free TSCuPc and SWNHs–TSCuPc in aqueous solution (Figure 1). Free TSCuPc shows two distinguishable absorption bands, peaked at 629 and 663 nm, corresponding to the presence of a dimer and a monomer of TSCuPc, respectively.[31] Upon complexation of SWNHs, the absorption band of the dimer peak largely disappears, whereas the absorption band of the monomer peak broadens and weakens, accompanying a red shift to ~700 nm. The phenomena indicate a strong π–π interaction between SWNHs and TSCuPc, which results in reduced aggregation of TSCuPc. More importantly, SWNHs–TSCuPc shows

stronger absorbance in IR and NIR, which favors photothermal conversion.

Subsequently, TEM measurements were performed to identify the morphological feature of the SWNHs−TSCuPc nanohybrid. As mentioned in previous works,[10−13] the closed spherical aggregations are clearly observed of the pristine SWNHs (Figure 2a), which are highly retained in the

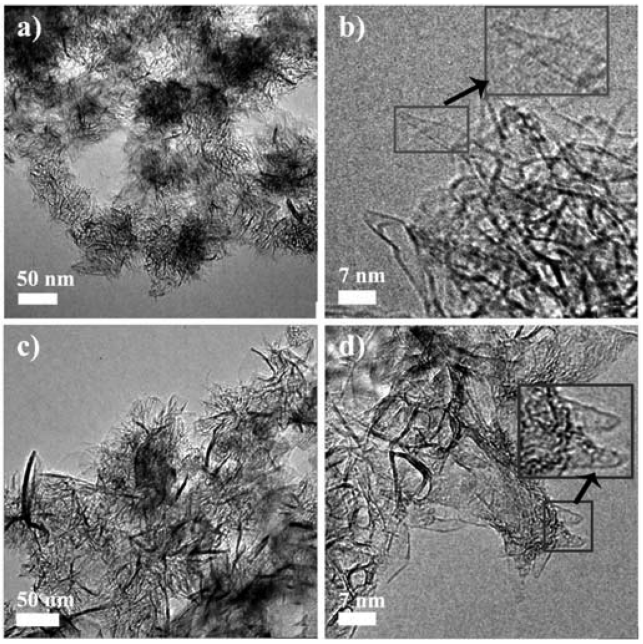

Figure 2. Representative TEM images of (a, b) pristine SWNHs and (c, d) SWNHs−TSCuPc nanohybrid. Insets in panels b and d show magnified views of the regions indicated.

SWNHs−TSCuPc nanohybrid (Figure 2c). Moreover, the integrity of tubular individual nanohorns before and after coating TSCuPc is also noticeable in the magnified images (see insets in Figures 2b and 2d), indicating that the surface functionalization with TSCuPc via noncovalent $\pi-\pi$ stacking produces insignificant damage to the intrinsic structures of SWNHs.

The formation of SWNHs−TSCuPc nanohybrid and the π-electron interaction between SWNHs and TSCuPc were characterized in detail by Raman spectra and X-ray photoelectron spectroscopy (XPS). As seen in Figure 3, Raman spectrum of pristine SWNHs shows two prominent bands at ~1341 cm^{-1} (D-band) and 1572 cm^{-1} (G-band) with almost the same intensity. The spectrum of the SWNHs−TSCuPc nanohybrid shows an increasing ratio between the intensities of the G- and D-bands, where the I_G/I_D ratio increases from 1.08 for pristine SWNHs to 1.33 for SWNHs−TSCuPc, suggesting a larger average sp^2 domain size and lower defect density of SWNHs structure in the hybrid.[32] Moreover, characteristic vibrational features of TSCuPc are observable in the Raman spectrum of SWNHs−TSCuPc nanohybrid, in which a new weak peak assigned to TSCuPc at 1531 cm^{-1} can be found, due to the peak overlapping between SWNHs and TSCuPc in SWNHs−TSCuPc nanohybrid. These results of Raman spectra further confirm the successful preparation of the SWNHs−TSCuPc hybrid.

XPS represents an effective technique for surface analysis, so the experiments of XPS were also employed to give evidence of

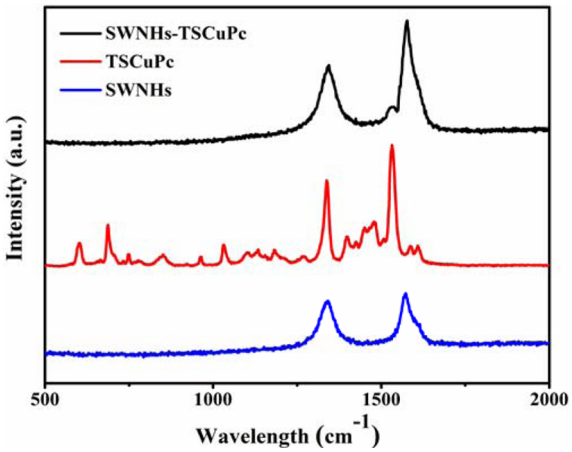

Figure 3. Raman spectra of SWNHs (bottom line), TSCuPc (middle line), and SWNHs−TSCuPc nanohybrid (upper line); λ_{exc} = 514 nm.

the SWNHs−TSCuPc nanohybrid. The XPS spectra of the hybrid show the photoelectrons collected from S 2p, Cu 2p, Na 1s core-levels, confirming the presence of TSCuPc at the surface of SWNHs (see Figure 4a). The C 1s core-level spectrum of the SWNHs−TSCuPc nanohybrid (Figure 4b) can be curve-fitted into five peak components with binding energies (BEs) of ~284.8, 285.6, 286.4, 287.5, and 290.5 eV, which are

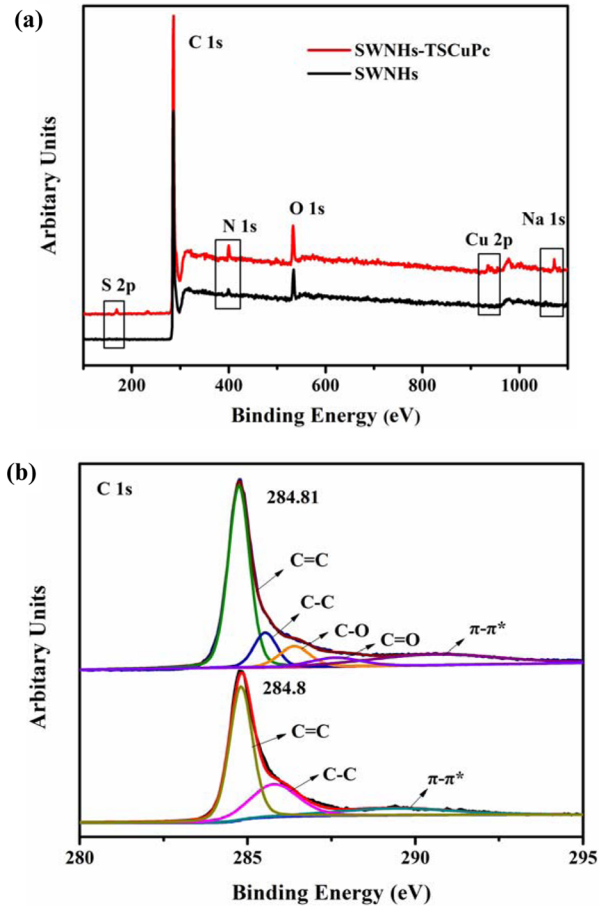

Figure 4. (a) XPS survey spectra of SWNHs (black spectrum) and SWNHs−TSCuPc nanohybrid (red spectrum). (b) High-resolution C 1s spectra of the SWNHs (bottom) and the SWNHs−TSCuPc nanohybrid (upper).

dx.doi.org/10.1021/am504860c | ACS Appl. Mater. Interfaces 2014, 6, 18008−18017

attributed to the sp^2 hybridized carbon, sp^3 hybridized carbon, C−O, C═O, and $\pi-\pi^*$ species, respectively.[33,34] It should be noted that a weak C−N/C−S component assigned to TSCuPc should be expected somewhere near ∼285.5 eV;[35,36] however, it is overshadowed by the stronger C−O line, and, therefore, it could not be resolved. The areal ratio of sp^2 and sp^3 hybridized carbon can be a measure of the defects formed during treatment, which has increased from ∼3.19 in SWNHs to ∼6.86 in SWNHs−TSCuPc (Figure 4b), corresponding to the result of Raman spectra that a larger average sp^2 domain size and lower defect density of SWNHs structure in the hybrid (Figure 3).

The binding energy is involved in the electron density around the nucleus, where the lower electronic density denotes the higher binding energy.[26] In the spectrum of the hybrid, the binding energy of the Cu $2p_{3/2}$ peak is increased by 0.71 eV, compared to that of TSCuPc alone (Figure 5a). Such a high binding energy shift indicates that the electronic density of the MPc ring decreased, owing to the charge transfer from TSCuPc to SWNHs. This result can be also proved by the N 1s spectrum. The N 1s peak of TSCuPc consists of two peaks separated by 1.2 eV, assigned to two groups of four N atoms in different chemical environments (namely, the outermost four nitrogens bond to carbon only and the four innermost nitrogens interact with the central copper cation).[37] In the composite spectral, the N peak shifts to higher binding energy by 0.2 eV, compared to that of free TSCuPc (Figure 5b). However, the S 2p spectrum in the hybrid has a global shift of 0.25 eV toward lower BEs (Figure 5c), probably bceause of the electron-withdrawing property of sufonate groups in TSCuPc.[38,39] Overall, the higher energy shifts in Cu 2p and N 1s are consistent with the reported charge-transfer phenomena.[30] From the surface composition (atomic percentage) determined by XPS (see Table S1 in the Supporting Information), the TSCuPc loading onto the skeleton of SWNHs is further calculated to be that one TSCuPc unit is conjugated for every 152 carbons of SWNHs, meaning that the SWNHs−TSCuPc nanohybrid is composed of 65% SWNHs and 35% TSCuPc.

The quantity of TSCuPc attached on the surface of SWNHs was further estimated by thermogravimetric analysis (TGA; see Figure 6). The curve of pristine SWNHs presents a weight loss of ∼6.5%, which may correspond to the destruction of the residual amorphous carbon. TSCuPc shows a characteristic thermogram with the first weight loss occurring before 260 °C, which may correspond to the desorption of adsorbed water;[27,40] the second occurs between 420 °C and 540 °C, and the third occurs between 580 °C and 730 °C. The SWNHs−TSCuPc nanohybrid exhibits some similarities to that of both SWNHs and TSCuPc, which confirms the presence of SWNHs and TSCuPc. From the weight loss and residue quantity at 850 °C, the weight percentage of TSCuPc in SWNHs−TSCuPc nanohybrid is determined to be 38% (namely, one TSCuPc unit per 134 carbons of SWNHs, which is consistent with the result obtained from XPS).

SWNHs are effective photothermal agents, producing fast and remarkable heat effects under laser irradiation.[14,19] To verify the efficacy of SWNHs−TSCuPc as a photothermal agent, we introduced a 650-nm laser at a power density of 3 W cm^{-2} to irradiate water, free TSCuPc, and SWNHs−TSCuPc for different irradiation times and used a thermal imager to record the temperature variation. As a control, the thermal signals of pure water show no obvious change (ΔT < 5 °C)

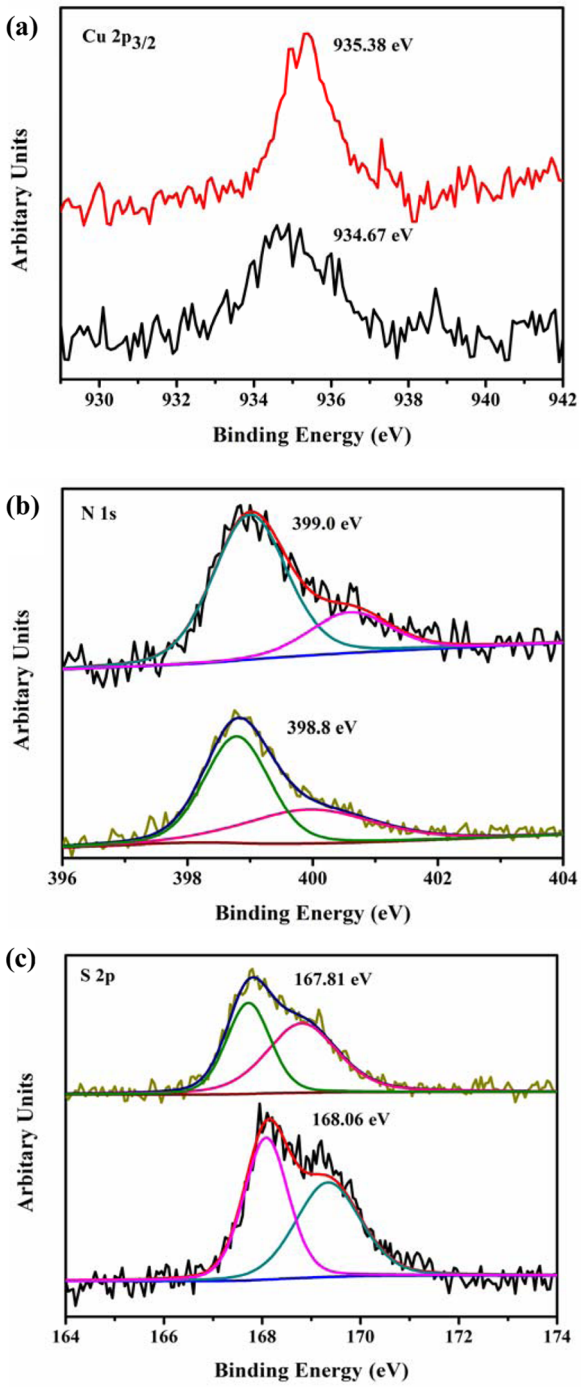

Figure 5. High-resolution spectra of (a) Cu $2p_{3/2}$, (b) N 1s, and (c) S 2p. For each set of core level spectra, the upper spectra belong to the SWNHs−TSCuPc nanohybrid and the lower spectra belong to TSCuPc.

after irradiation (see Figures 7c and 7d). In contrast, as the irradiation time increases, the color of the SWNHs−TSCuPc nanohybrid photothermal images continuously change from black to orange red, indicating a significant increase in temperature from 21 °C to 57 °C in 10 min (ΔT = 36 °C) (see Figures 7a and 7d). Under the same conditions, free TSCuPc also shows temperature increase (Figures 7b and 7d), which is smaller than that of the SWNHs−TSCuPc nanohybrid. Such an observation shows that free TSCuPc possesses photothermal conversion but is less efficient than the SWNHs−

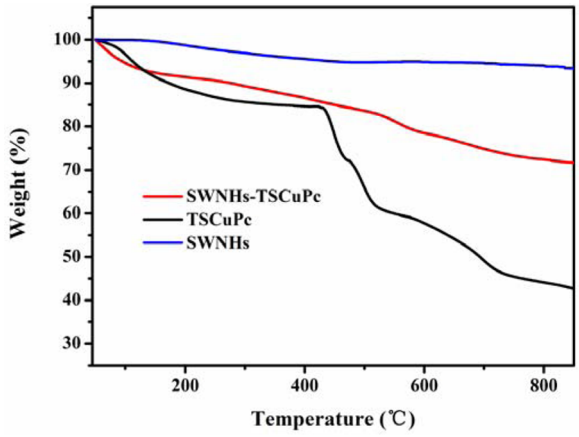

Figure 6. TGA curves of SWNHs, TSCuPc, and SWNHs–TSCuPc nanohybrid recorded at a rate of 10 °C/min under a N_2 atmosphere.

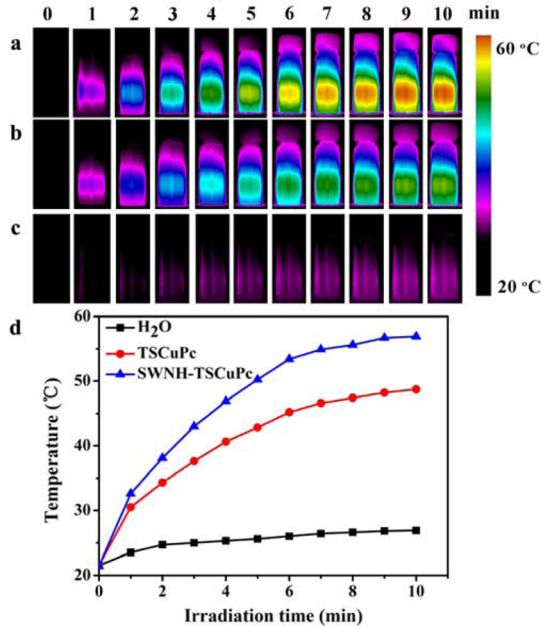

Figure 7. Photothermal images of (a) the SWNHs–TSCuPc nanohybrid solution (TSCuPc, 10 μg mL^{-1}; SWNHs, 16.5 μg mL^{-1}), (b) the TSCuPc solution (TSCuPc, 10 μg mL^{-1}), and (c) pure water exposed to a 650-nm laser (3 W cm^{-2}) for different time periods. (d) The corresponding time-dependent photothermal curves of the samples previously described in panels a–c.

TSCuPc nanohybrid. Unfortunately, we failed to record the photothermal images of the SWNHs, because of its insolubility in water. However, previous reports illustrated that SWNHs have high photothermal conversion efficiency and could act as an ideal PTT agent.[14,19,41,42] With all these results in hand, we can infer that not only do SWNHs contribute to the PTT effect, TSCuPc may also contribute to that when it coats on the surface of SWNHs upon exposure to a 650-nm laser. It is worth mentioning that the SWNHs–TSCuPc nanohybrid is heated to over 45 °C within 5 min, which is supposed for cancer cell killing.

It is generally accepted that photosensitizers transfer energy to the surrounding oxygen to generate $^1O_2$ when exposed selectively to light.[43,44] We primarily monitored the ability of free TSCuPc and SWNHs–TSCuPc to produce $^1O_2$ via a chemical method using anthracene-9,10-dipropionic acid disodium salt (ADPA) that can easily react with $^1O_2$ and be converted to a nonfluorescent endoperoxide.[45,46] Figure 8

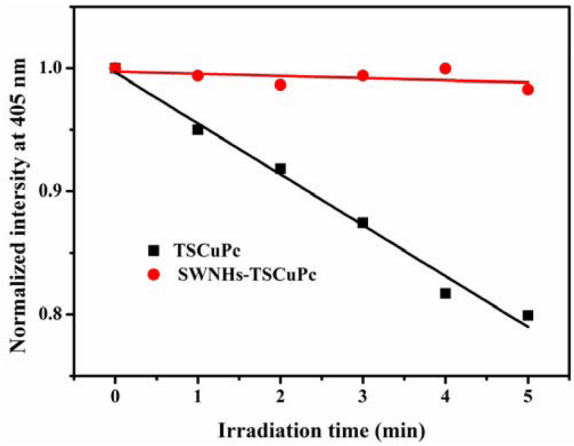

Figure 8. Time-dependent photobleaching of ADPA fluorescence at 405 nm as the generation of singlet oxygen upon exposure to a 650-nm laser (3 W cm^{-2}). The fluorescence intensity at 405 nm in all samples were normalized to corresponding samples at an irradiation time of 0 min.

shows the normalized fluorescence intensity of ADPA at 405 nm as a function of exposure time to a 650-nm laser irradiation. The fluorescence intensity of ADPA displays a continuous decrease within 5 min for free TSCuPc (Figure S1a in the Supporting Information and Figure 8), whereas it shows no fluorescence change for SWNHs–TSCuPc nanohybrid (Figure S1b in the Supporting Information and Figure 8). This means that $^1O_2$ can be generated via the laser irradiation of free TSCuPc but not the SWNHs–TSCuPc nanohybrid.

We further employed the electron paramagnetic resonance (EPR) spin trapping technique to investigate the more-detailed electron transfer process in the SWNHs–TSCuPc nanohybrid, where a common spin trap reagent (5,5-dimethyl-1-pyrroline-*N*-oxide, DMPO) was used to detect the $O_2^{\bullet -}$ or $OH^{\bullet}$. With the 650-nm laser irradiation of the SWNHs–TSCuPc nanohybrid, EPR signal of the adduct of DMPO with $OH^{\bullet}$ (DMPO–OH adduct) is detected, indicating the formation of $OH^{\bullet}$ (Figure 9a, blue line), whereas there is no DMPO–OH adduct signals without laser irradiation (Figure 9a, red line). Combining the EPR results and previous studies of electron transfer,[20,47] we inferred that when TSCuPc is excited by light, electrons transfer from the excited state of TSCuPc moiety to SWNHs and forms a charge separation state, giving SWNHs$^{\bullet -}$–TSCuPc$^{\bullet +}$, which further transfers the electrons to surrounding oxygen to generate superoxide radical anion ($O_2^{\bullet -}$) and then $OH^{\bullet}$.[48] The entire photochemical processes are illustrated in Scheme 2. It should be pointed out that no EPR signals of the adduct of DMPO with $O_2^{\bullet -}$ (DMPO–OOH adduct) is observed, which may be ascribed to the unstable and short-lived properties of DMPO–OOH that decomposes to DMPO–OH.[49,50] In addition, SWNHs may produce reactive oxygen species (ROS) upon laser irradiation, referring to a previous report.[51] To confirm this, we substituted an 808-nm (3 W cm^{-2}) laser for the 650-nm (3 W cm^{-2}) laser. Such an irradiation wavelength would impact only on the SWNHs without exciting TSCuPc to its excited state (see Figure S2 in the Supporting Information). With the irradiation of the 808-nm laser, a weak EPR signal of DMPO–OH adduct

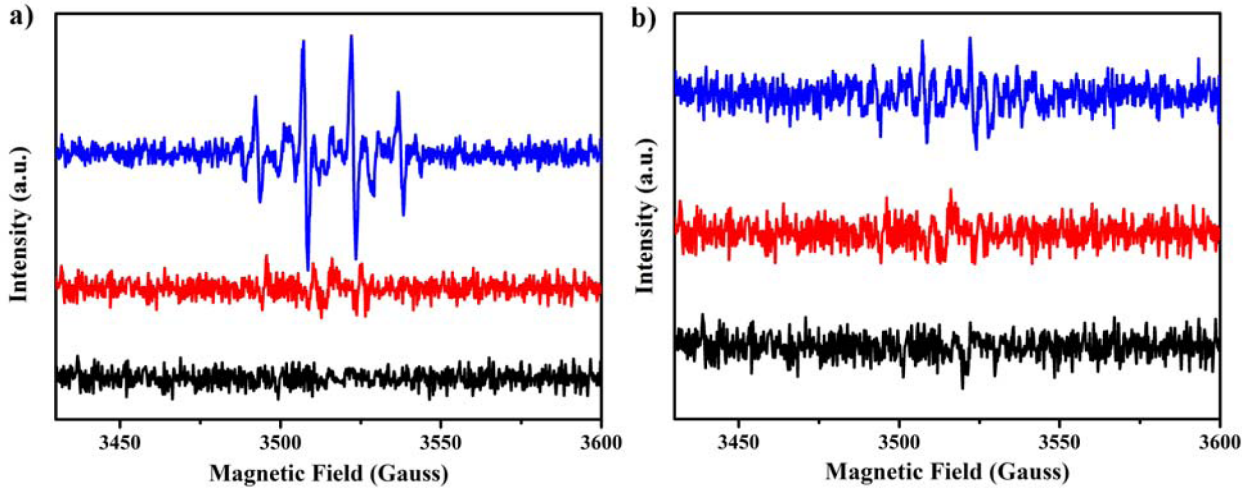

Figure 9. EPR spectra of DMPO with laser irradiation (black line), DMPO and SWNHs−TSCuPc without laser irradiation (red line), DMPO and SWNHs−TSCuPc nanohybrid with laser irradiation (blue line). Samples irradiated with (a) 650-nm laser (3 W cm^{-2}) and (b) 808-nm laser (3 W cm^{-2}).

Scheme 2. Schematic Illustration of the Possible Photoinduced Electron Transfer Process for SWNHs−TSCuPc Nanohybrid upon Irradiation by a 650-nm Laser

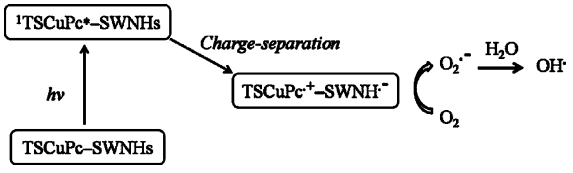

was also detected, demonstrating that SWNHs in the SWNHs−TSCuPc nanohybrid can generate $OH^{\bullet}$ (see Figure 9b). The presence of the ROS makes the SWNHs−TSCuPc nanohybrid ideally suitable for PDT.

***In Vitro* Cytotoxicity of SWNHs−TSCuPc Nanohybrid.** In order to evaluate the therapeutic effect of SWNHs−TSCuPc, cell viabilities with different treatments were measured. We first measured the dark toxicity of free TSCuPc and SWNHs−TSCuPc via a standard MTT assay *in vitro*, using human cervix cancer cells (HeLa). Different amounts of free TSCuPc and SWNHs−TSCuPc were added to HeLa cells that had incubated for 24 h. After 24 h of incubation, the cell viability was measured via MTT assay. As can be seen in Figure 10, the cell viabilities were >90%, even at the high concentration of 15 μg mL^{-1}, indicating that both free TSCuPc and SWNHs−TSCuPc have good biocompatibility and low cytotoxicity, which is consistent with the reports of Miyawaki and co-workers.[15,52]

Next, we tested the *in vitro* cytotoxicity of the PTT and PDT effect of the SWNHs−TSCuPc nanohybrid, where cells were incubated in a culture medium containing a series of concentrations of SWNHs−TSCuPc for 24 h, and then irradiated with a 650-nm laser. The standard MTT assay was used to determine the relative viabilities of cells at 24 h after various treatments. As a control, without TSCuPc or the SWNHs−TSCuPc nanohybrid, irradiation alone could not cause an obvious decrease in cell viability. However, when incubated with either TSCuPc or the SWNHs−TSCuPc nanohybrid, obvious cell death was observed (Figure 11). In addition, the SWNHs−TSCuPc nanohybrid with 650-nm laser irradiation induces significantly higher levels of cell death than that of free TSCuPc. The cell viability decreases to ~60% for

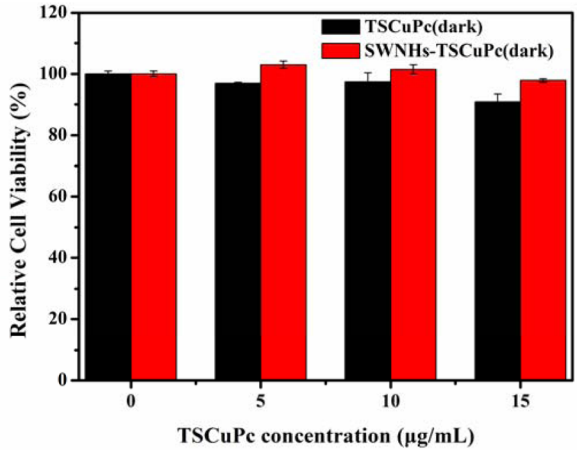

Figure 10. Dark cytotoxicity of free TSCuPc and the SWNHs−TSCuPc nanohybrid at a series of concentrations. [TSCuPc] = 0−15 μg mL^{-1}, SWNHs = 0−26.5 μg mL^{-1}.

free TSCuPc and to ~18% for the SWNHs−TSCuPc nanohybrid at the TSCuPc concentration of 10 μg mL^{-1} after being irradiated for 5 min, respectively. The phototherapy effect using the SWNHs−TSCuPc nanohybrid was much better than that of free TSCuPc. This clearly shows the combination of two different therapeutic modalities. In addition, an attempt was made to perform the cell viability experiment of pristine SWNHs with irradiation alone, but was restricted, because of insolubility of the SWNHs without any functionality. It should be noted that, although its lack of direct evidence of the phototherapy effect contributed by SWNHs, based on the previous studies on PTT of SWNHs,[14,19,41,42] we can infer that SWNHs indeed contribute to the phototherapy effect through photothermal conversion.

For the sake of visualizing the phototherapy efficacy of SWNHs−TSCuPc, the live/dead assay is used with calcein-AM and propidium iodide (PI) fluorescence dyes to identify living cells (green) and dead cells (red). As shown in Figure 12b and 12a, fluorescence images of green cells illustrated that the SWNHs−TSCuPc nanohybrid has negligible cytotoxicity for HeLa cells, incubated with the SWNHs−TSCuPc nanohybrid for 24 h (compared to the PBS control), in the absence of

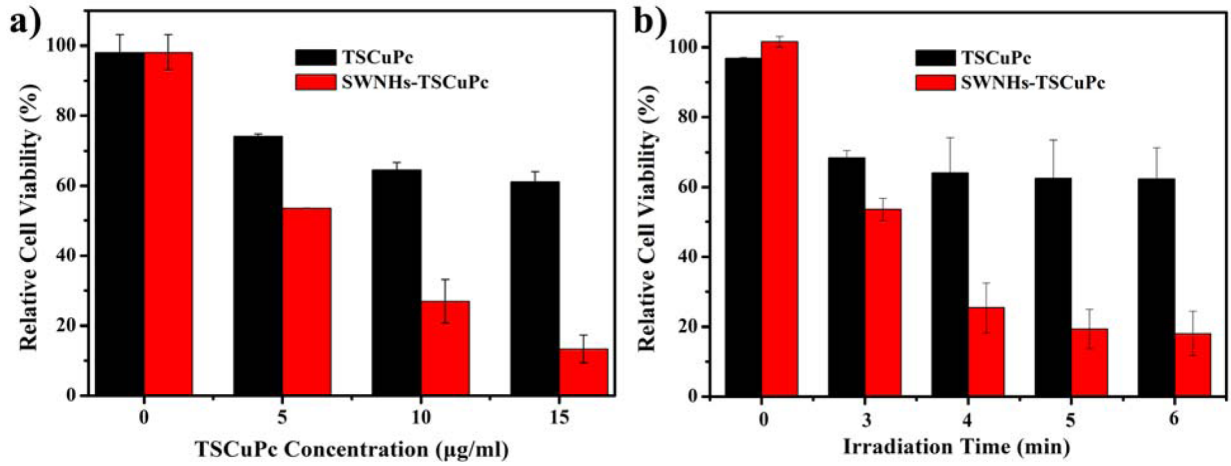

Figure 11. *In vitro* photodynamic and photothermal cancer cell killing: (a) cells treated with free TSCuPc or the SWNHs–TSCuPc nanohybrid at different concentrations (TSCuPc, 0–15 μg mL^{-1}; SWNHs, 0–26.5 μg mL^{-1}) with the same irradiation time using a 650-nm laser (3 W cm^{-2}, 5 min); (b) cells treated with free TSCuPc or the SWNHs–TSCuPc nanohybrid (TSCuPc, 10 μg mL^{-1}; SWNHs, 16.5 μg mL^{-1}), and then irradiated for various times.

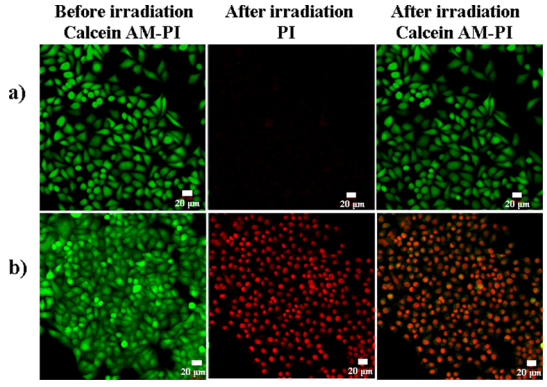

Figure 12. Confocal microscopy images of HeLa cells stained with calcein-AM (green, living cells) and PI (red, dead cells) after treatment with (a) PBS and (b) the SWNHs–TSCuPc nanohybrid (TSCuPc, 10 μg mL^{-1}; SWNHs, 16.5 μg mL^{-1}). These images were taken before and after irradiation with a 650-nm laser.

exposure to 650-nm light. Furthermore, fluorescence image shows red cells (Figure 12b) from HeLa cells incubated with the SWNHs–TSCuPc nanohybrid in the presence of exposure to a 650-nm laser *in situ* (compared to the PBS control, Figure 12a), provided evidence that the SWNHs–TSCuPc nanohybrid has significant phototherapy efficiency. The results obtained from fluorescence cells vitality assay (Figure 12) agree well with those tested from the MTT assay (see Figure 11).

For phototherapy, the cytotoxicity and phototherapy efficiency are two main factors that should be considered.[22,23] Based on the above results, the SWNHs–TSCuPc nanohybrid exhibits good biocompatibility. Moreover, the results also demonstrated that it has significant PTT/PDT phototherapy efficiency to HeLa cells *in vitro*. Hence, the as-prepared SWNHs–TSCuPc nanohybrid is a hopeful candidate for developing an efficient and biocompatible phototherapy agent. Nevertheless, much more effort, including its accumulation and distribution in tumor tissues, antitumor effectiveness *in vivo*, is needed to explore the potential applications and limitations of the SWNHs–TSCuPc nanohybrid.

4. CONCLUSION

In summary, we have successfully fabricated a water-soluble SWNHs–TSCuPc nanohybrid (SWNHs = single-walled carbon nanohorns, TSCuPc = tetrasodium salt copper phthalocyanine) for dual-modality photothermal therapy (PTT) and photodynamic therapy (PDT) via noncovalent π–π stacking interaction by a sonication method. In this nanosystem, SWNHs have proved to be the promising photosensitizer (PS) carriers and ideal PTT agents, while TSCuPc acts as a hydrophilic and PDT agent. It has been confirmed that the SWNHs–TSCuPc nanohybrid generates reactive oxygen species (ROS), not only from the photo-induced electron transfer process from TSCuPc to SWNHs, but also from SWNHs without exciting TSCuPc to its excited state. Moreover, the photothermal test proved that not only does SWNHs contribute to the PTT effect, TSCuPc may also contribute to that when it coats the surface of SWNHs upon exposure to a 650-nm laser. The cell viability test revealed that the combination of PTT and PDT shows much better cell killing efficacy *in vitro*. Therefore, our study provides a facile one-step method to develop an efficacious dual-modality SWNHs–TSCuPc nanoplatform for PTT/PDT cancer therapeutics.

■ ASSOCIATED CONTENT

Ⓢ Supporting Information

Surface composition (atomic percentage) determined by XPS, fluorescence spectra of ADPA mixed with free TSCuPc and SWNHs–TSCuPc. This material is available free of charge via the Internet at http://pubs.acs.org.

■ AUTHOR INFORMATION

Corresponding Authors

*Tel: (+86) 773-5846273. E-mail: xcshen@mailbox.gxnu.edu.cn (X.-C. Shen).

*Tel: (+86) 773-5846273. E-mail: hliang@gxnu.edu.cn (H. Liang).

Author Contributions

‡These authors contributed equally to this work.

Notes

The authors declare no competing financial interest.

■ ACKNOWLEDGMENTS

This work was supported by the Natural Science Foundation of China (Nos. 21161003 and 21364002); Guangxi Natural Science Foundation of China (Nos. 2013GXNSFGA019001, 2012GXNSFDA053007, and 2014GXNSFBA118038); the Program for New Century Excellent Talents in University of the Ministry of Education (No. NCET-13-0743); the Program for New Century National Hundred, Thousand and Ten Thousand Talent Project of Guangxi; the State Key Laboratory Cultivation Base for the Chemistry and Molecular Engineering of Medicinal Resources (Nos. CMEMR2012-A12, CMEMR2013-A8, and CMEMR2013-A13); the Program for Guangxi Scientific Research of Higher Education (No. YB2014052) and the Program for Key Scientific Research of Guangxi Normal University (No. 2013ZD005). We thank Prof. Hui Chao (Sun Yat-Sen University, China) and Haihua Pan (Zhejiang University, China) for their kind help with EPR tests.

■ REFERENCES

(1) Chung, C.; Kim, Y.-K.; Shin, D.; Ryoo, S.-R.; Hong, B. H.; Min, D.-H. Biomedical Applications of Graphene and Graphene Oxide. *Acc. Chem. Res.* **2013**, *46*, 2211−2224.

(2) Chen, Z.; Ma, L.; Liu, Y.; Chen, C. Applications of Functionalized Fullerenes in Tumor Theranostics. *Theranostics* **2012**, *2*, 238−250.

(3) De Volder, M. F.; Tawfick, S. H.; Baughman, R. H.; Hart, A. J. Carbon Nanotubes: Present and Future Commercial Applications. *Science* **2013**, *339*, 535−539.

(4) Song, Y.; Qu, K.; Zhao, C.; Ren, J.; Qu, X. Graphene Oxide: Intrinsic Peroxidase Catalytic Activity and Its Application to Glucose Detection. *Adv. Mater.* **2010**, *22*, 2206−2210.

(5) Calvaresi, M.; Zerbetto, F. The Devil and Holy Water: Protein and Carbon Nanotube Hybrids. *Acc. Chem. Res.* **2013**, *46*, 2454−2463.

(6) Bianco, A. Carbon Nanotubes for the Delivery of Therapeutic Molecules. *Expert Opin. Drug Delivery* **2004**, *1*, 57−65.

(7) Liu, Z.; Fan, A. C.; Rakhra, K.; Sherlock, S.; Goodwin, A.; Chen, X.; Yang, Q.; Felsher, D. W.; Dai, H. Supramolecular Stacking of Doxorubicin on Carbon Nanotubes for In Vivo Cancer Therapy. *Angew. Chem., Int. Ed.* **2009**, *48*, 7668−7672.

(8) Liu, Z.; Robinson, J. T.; Sun, X.; Dai, H. PEGylated Nanographene Oxide for Delivery of Water-Insoluble Cancer Drugs. *J. Am. Chem. Soc.* **2008**, *130*, 10876−10877.

(9) Cheng, Q.; Wu, M.; Li, M.; Jiang, L.; Tang, Z. Ultratough Artificial Nacre Based on Conjugated Cross-linked Graphene Oxide. *Angew. Chem., Int. Ed.* **2013**, *125*, 3838−3843.

(10) Zhu, S.; Xu, G. Single-Walled Carbon Nanohorns and Their Applications. *Nanoscale* **2010**, *2*, 2538−2549.

(11) Iijima, S.; Yudasaka, M.; Yamada, R.; Bandow, S.; Suenaga, K.; Kokai, F.; Takahashi, K. Nano-Aggregates of Single-Walled Graphitic Carbon Nano-Horns. *Chem. Phys. Lett.* **1999**, *309*, 165−170.

(12) Kasuya, D.; Yudasaka, M.; Takahashi, K.; Kokai, F.; Iijima, S. Selective Production of Single-Wall Carbon Nanohorn Aggregates and Their Formation Mechanism. *J. Phys. Chem. B* **2002**, *106*, 4947−4951.

(13) Li, N.; Wang, Z.; Zhao, K.; Shi, Z.; Gu, Z.; Xu, S. Synthesis of Single-Wall Carbon Nanohorns by Arc-Discharge in Air and Their Formation Mechanism. *Carbon* **2010**, *48*, 1580−1585.

(14) Chen, D.; Wang, C.; Jiang, F.; Liu, Z.; Shu, C.; Wan, L.-J. In Vitro and In Vivo Photothermally Enhanced Chemotherapy by Single-Walled Carbon Nanohorns as a Drug Delivery System. *J. Mater. Chem. B* **2014**, *2*, 4726−4732.

(15) Miyawaki, J.; Yudasaka, M.; Azami, T.; Kubo, Y.; Iijima, S. Toxicity of Single-Walled Carbon Nanohorns. *ACS Nano* **2008**, *2*, 213−226.

(16) Xiao, Z.; Ye, G.; Liu, Y.; Chen, S.; Peng, Q.; Zuo, Q.; Ding, L. Pushing Fullerene Absorption into the Near-IR Region by Conjugately Fusing Oligothiophenes. *Angew. Chem., Int. Ed.* **2012**, *51*, 9038−9041.

(17) Huang, P.; Xu, C.; Lin, J.; Wang, C.; Wang, X.; Zhang, C.; Zhou, X.; Guo, S.; Cui, D. Folic Acid-Conjugated Graphene Oxide Loaded with Photosensitizers for Targeting Photodynamic Therapy. *Theranostics* **2011**, *1*, 240−250.

(18) Lee, D. J.; Park, S. Y.; Oh, Y. T.; Oh, N. M.; Oh, K. T.; Youn, Y. S.; Lee, E. S. Preparation of Chlorine e6-Conjugated Single-Wall Carbon Nanotube for Photodynamic Therapy. *Macromol. Res.* **2011**, *19*, 848−852.

(19) Zhang, M.; Murakami, T.; Ajima, K.; Tsuchida, K.; Sandanayaka, A. S.; Ito, O.; Iijima, S.; Yudasaka, M. Fabrication of ZnPc/Protein Nanohorns for Double Photodynamic and Hyperthermic Cancer Phototherapy. *Proc. Natl. Acad. Sci. U. S. A.* **2008**, *105*, 14773−14778.

(20) Sandanayaka, A. S.; Ito, O.; Zhang, M.; Ajima, K.; Iijima, S.; Yudasaka, M.; Murakami, T.; Tsuchida, K. Photoinduced Electron Transfer in Zinc Phthalocyanine Loaded on Single-Walled Carbon Nanohorns in Aqueous Solution. *Adv. Mater.* **2009**, *21*, 4366−4371.

(21) Dolmans, D. E. G. J.; Fukumura, D.; Jain, R. K. Photodynamic Therapy for Cancer. *Nat. Rev. Cancer* **2003**, *3*, 380−387.

(22) Sharman, W. M.; Allen, C. M.; Van Lier, J. E. Photodynamic Therapeutics: Basic Principles and Clinical Applications. *Drug Discovery Today* **1999**, *4*, 507−517.

(23) Shibu, E. S.; Hamada, M.; Murase, N.; Biju, V. Nanomaterials Formulations for Photothermal and Photodynamic Therapy of Cancer. *J. Photochem. Photobiol., C* **2013**, *15*, 53−72.

(24) Ma, X.; Sreejith, S.; Zhao, Y. Spacer Intercalated Disassembly and Photodynamic Activity of Zinc Phthalocyanine Inside Nanochannels of Mesoporous Silica Nanoparticles. *ACS Appl. Mater. Interfaces* **2013**, *5*, 12860−12868.

(25) Dhami, S.; Phillips, D. Comparison of the Photophysics of an Aggregating and Non-Aggregating Aluminium Phthalocyanine System Incorporated into Unilamellar Vesicles. *J. Photochem. Photobiol., A* **1996**, *100*, 77−84.

(26) Hatton, R. A.; Blanchard, N. P.; Stolojan, V.; Miller, A. J.; Silva, S. R. P. Nanostructured Copper Phthalocyanine-Sensitized Multiwall Carbon Nanotube Films. *Langmuir* **2007**, *23*, 6424−6430.

(27) Zeng, J.-Q.; Sun, S.-N.; Zhong, J.-P.; Li, X.-F.; Wang, R.-X.; Wu, L.-N.; Wang, L.; Fan, Y.-J. Pd Nanoparticles Supported on Copper Phthalocyanine Functionalized Carbon Nanotubes for Enhanced Formic Acid Electrooxidation. *Int. J. Hydrogen Energy* **2014**, *39*, 15928−15936.

(28) Zhong, J.-P.; Fan, Y.-J.; Wang, H.; Wang, R.-X.; Fan, L.-L.; Shen, X.-C.; Shi, Z.-J. Copper Phthalocyanine Functionalization of Graphene Nanosheets as Support for Platinum Nanoparticles and Their Enhanced Performance Toward Methanol Oxidation. *J. Power Sources* **2013**, *242*, 208−215.

(29) Zhang, Y.-Q.; Fan, Y.-J.; Cheng, L.; Fan, L.-L.; Wang, Z.-Y.; Zhong, J.-P.; Wu, L.-N.; Shen, X.-C.; Shi, Z.-J. A Novel Glucose Biosensor Based on the Immobilization of Glucose Oxidase on Layer-by-Layer Assembly Film of Copper Phthalocyanine Functionalized Graphene. *Electrochim. Acta* **2013**, *104*, 178−184.

(30) Chunder, A.; Pal, T.; Khondaker, S. I.; Zhai, L. Reduced Graphene Oxide/Copper Phthalocyanine Composite and Its Opto-electrical Properties. *J. Phys. Chem. C* **2010**, *114*, 15129−15135.

(31) Brożek-Płuska, B.; Szymczyk, I.; Abramczyk, H. Raman Spectroscopy of Phthalocyanines and Their Sulfonated Derivatives. *J. Mol. Struct.* **2005**, *744*, 481−485.

(32) Mensing, J. P.; Kerdcharoen, T.; Sriprachuabwong, C.; Wisitsoraat, A.; Phokharatkul, D.; Lomas, T.; Tuantranont, A. Facile Preparation of Graphene−Metal Phthalocyanine Hybrid Material by Electrolytic Exfoliation. *J. Mater. Chem.* **2012**, *22*, 17094−17099.

(33) Díaz, J.; Paolicelli, G.; Ferrer, S.; Comin, F. Separation of the sp^3 and sp^2 Components in the C1s Photoemission Spectra of Amorphous Carbon Films. *Phys. Rev. B* **1996**, *54*, 8064−8069.

(34) McFeely, F. R.; Kowalczyk, S. P.; Ley, L.; Cavell, R. G.; Pollak, R. A.; Shirley, D. A. X-ray Photoemission Studies of Diamond, Graphite, and Glassy Carbon Valence Bands. *Phys. Rev. B* **1974**, *9*, 5268−5278.

(35) Vizuete, M.; Gómez-Escalonilla, M. J.; Fierro, J. L. G.; Yudasaka, M.; Iijima, S.; Vartanian, M.; Iehl, J.; Nierengarten, J.-F.; Langa, F. A Soluble Hybrid Material Combining Carbon Nanohorns and C_{60}. *Chem. Commun.* **2011**, *47*, 12771−12773.

(36) Xu, L. Q.; Yang, W. J.; Neoh, K.-G.; Kang, E.-T.; Fu, G. D. Dopamine-Induced Reduction and Functionalization of Graphene Oxide Nanosheets. *Macromolecules* **2010**, *43*, 8336−8339.
(37) Zheng, D.; Gao, Z.; He, X.; Zhang, F.; Liu, L. Surface and Interface Analysis for Copper Phthalocyanine (CuPc) and Indium-Tin-Oxide (ITO) Using X-ray Photoelectron Spectroscopy (XPS). *Appl. Surf. Sci.* **2003**, *211*, 24−30.
(38) Graupner, R.; Abraham, J.; Vencelová, A.; Seyller, T.; Hennrich, F.; Kappes, M. M.; Hirsch, A.; Ley, L. Doping of Single-Walled Carbon Nanotube Bundles by Brønsted Acids. *Phys. Chem. Chem. Phys.* **2003**, *5*, 5472−5476.
(39) Su, Q.; Pang, S.; Alijani, V.; Li, C.; Feng, X.; Müllen, K. Composites of Graphene with Large Aromatic Molecules. *Adv. Mater.* **2009**, *21*, 3191−3195.
(40) Zhang, M.; Shao, C.; Guo, Z.; Zhang, Z.; Mu, J.; Cao, T.; Liu, Y. Hierarchical Nanostructures of Copper(II) Phthalocyanine on Electrospun TiO_2 Nanofibers: Controllable Solvothermal-Fabrication and Enhanced Visible Photocatalytic Properties. *ACS Appl. Mater. Interfaces* **2011**, *3*, 369−377.
(41) Sawdon, A.; Weydemeyer, E.; Peng, C.-A. Tumor Photothermolysis: Using Carbon Nanomaterials for Cancer Therapy. *Eur. J. Nanomed.* **2013**, *5*, 131−140.
(42) Whitney, J. R.; Sarkar, S.; Zhang, J.; Do, T.; Young, T.; Manson, M. K.; Campbell, T. A.; Puretzky, A. A.; Rouleau, C. M.; More, K. L.; Geohegan, D. B.; Rylander, C. G.; Dorn, H. C.; Rylander, M. N. Single Walled Carbon Nanohorns as Photothermal Cancer Agents. *Lasers Surg. Med.* **2011**, *43*, 43−51.
(43) Dougherty, T. J.; Gomer, C. J.; Henderson, B. W.; Jori, G.; Kessel, D.; Korbelik, M.; Moan, J.; Peng, Q. Photodynamic Therapy. *J. Natl. Cancer Inst.* **1998**, *90*, 889−905.
(44) O'Connor, A. E.; Gallagher, W. M.; Byrne, A. T. Porphyrin and Nonporphyrin Photosensitizers in Oncology: Preclinical and Clinical Advances in Photodynamic Therapy. *Photochem. Photobiol.* **2009**, *85*, 1053−1074.
(45) Tang, W.; Xu, H.; Kopelman, R.; Philbert, M. A. Photodynamic Characterization and In Vitro Application of Methylene Blue-Containing Nanoparticle Platforms. *Photochem. Photobiol.* **2005**, *81*, 242−249.
(46) Yan, F.; Kopelman, R. The Embedding of Meta-tetra (Hydroxyphenyl)-Chlorin into Silica Nanoparticle Platforms for Photodynamic Therapy and Their Singlet Oxygen Production and pH-Dependent Optical Properties. *Photochem. Photobiol.* **2003**, *78*, 587−591.
(47) Zhang, X.-F.; Xi, Q. A Graphene Sheet as an Efficient Electron Acceptor and Conductor for Photoinduced Charge Separation. *Carbon* **2011**, *49*, 3842−3850.
(48) Nakanishi, I.; Fukuzumi, S.; Konishi, T.; Ohkubo, K.; Fujitsuka, M.; Ito, O.; Miyata, N. DNA Cleavage via Superoxide Anion Formed in Photoinduced Electron Transfer from NADH to γ-Cyclodextrin-Bicapped C_{60} in an Oxygen-Saturated Aqueous Solution. *J. Phys. Chem. B* **2002**, *106*, 2372−2380.
(49) Lee, J.; Yamakoshi, Y.; Hughes, J. B.; Kim, J.-H. Mechanism of C_{60} Photoreactivity in Water: Fate of Triplet State and Radical Anion and Production of Reactive Oxygen Species. *Environ. Sci. Technol.* **2008**, *42*, 3459−3464.
(50) Lipovsky, A.; Tzitrinovich, Z.; Friedmann, H.; Applerot, G.; Gedanken, A.; Lubart, R. EPR Study of Visible Light-Induced ROS Generation by Nanoparticles of ZnO. *J. Phys. Chem. C* **2009**, *113*, 15997−16001.
(51) Biju, V. Chemical Modifications and Bioconjugate Reactions of Nanomaterials for Sensing, Imaging, Drug Delivery and Therapy. *Chem. Soc. Rev.* **2014**, *43*, 744−764.
(52) Murakami, T.; Ajima, K.; Miyawaki, J.; Yudasaka, M.; Iijima, S.; Shiba, K. Drug-Loaded Carbon Nanohorns: Adsorption and Release of Dexamethasone *In Vitro*. *Mol. Pharmaceutics* **2004**, *1*, 399−405.